A full-aperture anisotropic eikonal solver for quasi-P traveltimes

Jianliang Qian, University of Minnesota, William W. Symes, Rice University, and Joe A. Dellinger, BP-Amoco*

Summary

The quasi-P traveltimes in general anisotropic media satisfy a nonlinear first-order PDE which is implicitly defined by quasi-P slowness surface. Given a point source as an initial condition, this nonlinear PDE is a stationary eikonal equation. The paraxial formulation for quasi-P eikonal equations provides a framework for obtaining high order accuracy by using explicit finite difference methods. A full-aperture anisotropic eikonal solver results from combining the paraxial formulations in different marching directions with the down-n-out and post sweeping techniques. Numerical computations for arbitrary anisotropic quasi-P traveltimes illustrate the accuracy and efficiency of the proposed anisotropic eikonal solver.

Introduction

Anisotropic traveltimes are essential in seismic data processing (de Hoop et al., 1999). The traveltime solvers roughly fall into two categories: ray-tracing based (Cerveny, 1972) and finite-difference eikonal based (Vidale, 1988; van Trier and Symes, 1991; Dellinger, 1991; Qin and Schuster, 1993; Schneider et al., 1992; Dellinger and Symes, 1997; Popovici and Sethian, 1997; Kim and Cook, 1999; Kim, 1999; Qian et al., 1999). Although the finite-difference eikonal solvers are well developed for isotropic media, no detailed algorithms are available for constructing finite-difference eikonal solvers in general anisotropic media.

Dellinger and Symes (1991; 1997) proposed a down-n-out (DNO) approach for computing the full-aperture anisotropic traveltimes, but they did not give full algorithmic details. For isotropic media, Kim and Cook (1999) improved the stability of DNO by applying post sweeping technique in different marching directions to the traveltime field after the DNO marching. However, in anisotropic media, the slowness vector can not serve as the indicator of the ray direction directly; therefore, unlike in the isotropic media, it is no longer easy to control the marching directions (and ray directions) by simply using the slowness vector. Kim (1999) has discussed the local convexity of the wavefront in transversely isotropic media and used the property to determine the upwind direction in his eikonal solvers. Actually, the quasi-P slowness surface is strictly convex in general anisotropic media as shown by Musgrave (Musgrave, 1970, 92); therefore, Qian and Symes (1999) used this convexity to construct the paraxial eikonal equation for quasi-P waves in general anisotropic media and demonstrated a simple application to transversely isotropic media with vertical symmetry axis. This paraxial formulation naturally provides a framework for constructing eikonal solvers in different marching directions and thus for different ray directions. By incorporating DNO and Fermat's principle based post sweeping (PS) iterative update, a full-aperture eikonal solver computes quasi-P traveltimes efficiently and accurately.

The point of departure is the formualtion of paraxial eikonal equations for quasi-P waves. We give the full details for computing the desired paraxial Hamiltonian; a second-order essentially nonoscillatory (ENO) Godunov scheme enhanced by DNO and PS update is used to solve the eikonal equation. A shooting method is designed to generate the traveltime from a source point to a specified point. Some examples illustrate the accuracy of the proposed algorithms.

The quasi-P paraxial eikonal equation

High-frequency approximation to the elastic wave equation leads to the Christoffel polynomial equation (Musgrave, 1970, 84),

$$G(p_1, p_2, p_3) \quad = \quad 0, \tag{1}$$

in which $\mathbf{p} = \nabla\tau$ is the slowness vector, τ is the traveltime or phase of the mode. Equation (1) is sextic and characterizes the slowness surface which consists of three sheets corresponding to three wave modes; see Figure 1.

We are interested in the downgoing wave propagation. By using convexity of quasi-P slowness surface (Musgrave, 1970, 92), Qian and Symes (1999) first introduced a function H to pick out the part of quasi-P slowness surface which corresponds to the downgoing rays; then they modified the function H to obtain a paraxial Hamiltonian H_Δ, which is defined in the whole horizontal slowness space. Finally, they obtained the **paraxial eikonal equation**

$$\frac{\partial\tau}{\partial x_3} \quad = \quad H_\Delta\left(\mathbf{x}, \frac{\partial\tau}{\partial x_1}, \frac{\partial\tau}{\partial x_2}\right). \tag{2}$$

We refer the reader to Qian and Symes (1999) for technical details.

Compute paraxial Hamiltonian H_Δ

We have to devise some algorithms to compute the paraxial Hamiltonian H_Δ. The inner sheet of the slowness surface (1) is convex and corresponds to quasi-P wave mode. By introducing the planar polar coordinates, we transform this sextic polynomial equation to a sextic polynomial equation in p and p_3 for each planar angle ϕ; namely, we have a two-dimensional problem to deal with now.

Suppose that the two-dimensional slowness surface is given by

$$F(p_1, p_3) \quad = \quad 0, \tag{3}$$

where F is a sextic or quartic polynomial in p_1 and p_3, respectively. Specifically, in this section we assume that F is a sextic polynomial in p_1 and p_3; the quartic case can be treated similarly. The related ray equations are

$$v_g^1 = \frac{dx_1}{dt} \quad = \quad \left(p_1 \frac{\partial F}{\partial p_1} + p_3 \frac{\partial F}{\partial p_3} \right)^{-1} \frac{\partial F}{\partial p_1}, \tag{4}$$

$$v_g^3 = \frac{dx_3}{dt} \quad = \quad \left(p_1 \frac{\partial F}{\partial p_1} + p_3 \frac{\partial F}{\partial p_3} \right)^{-1} \frac{\partial F}{\partial p_3}. \tag{5}$$

For arbitrary p_1^* there are four possiblities for the roots p_3 of the sextic polynomial equation $F(p_1^*, p_3) = 0$: (1) no real roots at all; (2) two real roots; (3) four real roots; (4) six real roots. We are especially interested in case (4) since this means that among the six real roots there are two roots **possibly** corresponding to the quasi-P wave. Because the quasi-P slowness surface, denoted as $\mathbf{S}$, is convex, separated from and nested inside other two ovoid surfaces, the straight line $p_1 = p_1^*$ has two intersection points with $\mathbf{S}$ **if** $(p_1 = p_1^*, 0)$ is inside the domain enclosed by the quasi-P slowness surface. This **if** condition is important because it is possible that no roots among the six real roots correspond to the quasi-P wave; see the dashed line in Figure 1 which corresponds to cusps. Since the origin is in the domain enclosed by $\mathbf{S}$, p_1^* can be taken small enough to guarantee that the straight line $p_1 = p_1^*$ has six real intersection points with the solwness surface, among which two are on the quasi-P slowness surface $\mathbf{S}$. The six real roots can be sorted into ascending order; moreover, the third and fourth roots correspond to the two intersection points with the quasi-P slowness surface.

Because $\mathbf{S}$ is strictly convex and closed, there are two extreme points at which $F = 0$ and $\dfrac{\partial F}{\partial p_3} = 0$, which correspond to the two horizontal rays (pointing to the positive and negative directions). To locate such points, we need two sets of intersection points $(p_1^*, p_3^{\rm up})$ and $(p_1^*, p_3^{\rm dn})$, which can be computed with p_1^* chosen as positive and negative numbers near zero, respectively.

Assuming that $(p_1^*, p_3^{\rm up})$ and $(p_1^*, p_3^{\rm dn})$ on the quasi-P slowness surface $\mathbf{S}$ are known, we can find on $\mathbf{S}$ an extreme point $(p_1^{\rm m}, p_3^{\rm m})$ which corresponds to the stationary point of function $p_1 = f(p_3)$ defined by the graph $\{(p_1, p_3) : p_1 \geq p_1^*, p_3^{\rm dn} \leq p_3 \leq p_3^{\rm up}, F(p_1, p_3) = 0\}$. Since the function f is convex, its derivative is monotonic; therefore, a typical nonlinear iterative solver can be used to compute the unique stationary point, such as Newton's method. The above stationary point is also of critical importance in the adaptation of upwind finite-difference schemes from numerical methods for Hamilton-Jacobi equations, because in that setting it is called the sonic point, needed to decide the upwinding direction.

Once the two extreme points (p_1^+, p_3^+) and (p_1^-, p_3^-), corresponding to the two horizontal rays, are located, it is easy to see that all $p_1 \in ((1-\Delta)p_1^-, (1-\Delta)p_1^+)$ give rise to downgoing rays and upgoing quasi-P rays by utilizing different roots of p_3, where Δ in between 0 and 1 is a user-specified paraxial parameter for depth direction marching. For $p_1 \leq (1-\Delta)p_1^-$, we simply set the paraxial Hamiltonian $H_\Delta(p_1) = H((1-\Delta)p_1^-)$; similar treatment for $p_1 \geq (1-\Delta)p_1^+$.

Upwind finite difference schemes

To solve the paraxial eikonal equation (2) along depth direction, we use a second-order ENO-Godunov scheme. By introducing the planar polar coodinates, we essentially reduce one dimension, and thus we only need to deal with a two dimensional problem.

Given mesh sizes Δx_1 and Δx_3, we denote τ_m^n as the numerical approximation to the viscosity solution $\tau(x_1^m, x_3^n)$ of equation (2) at the grid point (x_1^m, x_3^n). Define the backward $(-)$ and forward $(+)$ first order difference quotient approximations to the left and right derivatives of $\tau(x_1, x_3)$ at the location (x_1^m, x_3^n) with respect to x_1 as $D_{x_1}^{\pm}\tau_m^n = \pm(\Delta x_1)^{-1}(\tau_{m\pm1}^n - \tau_m^n)$.

The second-order ENO refinement to $\dfrac{\partial \tau}{\partial x_1}$ (Osher and Shu, 1991) are

$$D_{x_1}^{\pm,2}\tau_m^n = D_{x_1}^{\pm}\tau_m^n \mp \frac{1}{2}\Delta x_1 \, m(D_{x_1}^{\pm} D_{x_1}^{\pm}\tau_m^n, D_{x_1}^{-} D_{x_1}^{+}\tau_{m,k}^n),$$

with $m(x,y) = \min(\max(x,0), \max(y,0)) + \max(\min(x,0), \min(y,0))$.

So a second-order ENO Runge-Kutta scheme for equation (2) can be formulated as (Osher and Shu, 1991)

$$\tau_m^{n_0} = \tau_m^n + \Delta x_3^{\rm cfl} H_\Delta^{\rm G}\left(D_{x_1}^{-,2}\tau_m^n, D_{x_1}^{+,2}\tau_m^n\right),$$

$$\tau_m^{n+1} = \frac{1}{2}\left(\tau_m^n + \tau_m^{n_0} + \Delta x_3^{\rm cfl} H_\Delta^{\rm G}\left(D_{x_1}^{-,2}\tau_m^{n_0}, D_{x_1}^{+,2}\tau_m^{n_0}\right)\right),$$

where the Godunov flux $H_\Delta^{\rm G}$ is defined by

$$H_\Delta^{\rm G}(u^-, u^+) = \begin{cases} \max\limits_{u^- \leq u \leq v^+} H_\Delta(u), \text{if } u^- \leq u+; \\ \min\limits_{u^+ \leq u \leq v^-} H_\Delta(u), \text{ else.} \end{cases} \tag{6}$$

The depth step $\Delta x_3{}^{\rm cfl}$ must satisfy the CFL stability condition, which amounts to checking CFL on the boundary since H_Δ is concave (Qian and Symes, 1999).

If the sonic point is at $p_1 = 0$, which is true for isotropic and VTI eikonal equations, the Godunov flux function can be simplified; see (Kim and Cook, 1999; Qian and Symes, 1999). In general, we have to use the methodology stated above to compute the sonic points (extreme points). In the concave case, this sonic point is unique on the downgoing part of the quasi-P slowness surface; therefore, the Godunov flux can be elegantly implemented.

Analytical traveltime solver

Supposing that we have two extreme points (p_1^+, p_3^+) and (p_1^-, p_3^-), the ray tracing equation (4) and (5) says that the outward normals at these two extreme points correspond to the rays which point to the horizontal directions (positive or negative, respectively). Once realizing this, we can design a shooting method to compute the traveltime from the source point to a specific point in homogeneous anisotropic media. The idea is, given a group angle, finding the corresponding slowness vector by a nonlinear iterative solver; then the group velocity gives the desired traveltime.

Down-N-Out and post sweeping update

The above methodology and algorithms can be used to compute the paraxial Hamiltonian along any prefered marching direction, such as positive and negative x, y, z directions, respectively. So the DNO approach (Dellinger and Symes, 1997) and PS update (Schneider et al., 1992; Kim and Cook, 1999) can be naturally incorporated into the paraxial eikonal solver to get the full-aperture traveltime field.

However, unlike isotropic eikonal solvers, we have to be careful in prescribing appropriate aperture parameters Δ in different marching directions so that the effective aperture of marching directions are overlapped. Based on this observation, Fermat's principle is the foundation for the post sweeping process.

Numerical experiments

To give some idea of the accuracy obtainable with algorithms detailed in the preceding sections, we demonstrate the algorithms on a two-dimensional transversely isotropic medium with an inclined symmetry axis (ITI). The ITI slowness surface equation can be obtained by rotating the corresponding slowness surface for the TI media with vertical symmetry axis (VTI) (Kim, 1999). Then we solve the eikonal equation (2) by using the second-order upwind scheme and DNO-PS approach.

First we have to address the traveltime initialization. Due to the singularity of the traveltime field at the source which will lead to the contamination of global numerical accuracy, to initialize the traveltime we have to use some special techniques, such as the adaptive-grid method (Qian et al., 1999), or the local uniform mesh refinement (Kim and Cook, 1999). However, here we assume a homogeneous layer near the source and start the finite-difference scheme some distance away from the source; namely, we use the analytical traveltime solver to assign directly the traveltime at every grid point on a surface away from the source.

Table 1: Convergence order of the scheme

Δx_1	Abs.Err$(\tau, \Delta x_1)$(s)	Rel.Err$(\tau, \Delta x_1)$	α
0.04	0.0022	0.0049	
0.02	6.8005e-04	0.0015	1.6938
0.01	1.8129e-04	4.0871e-04	1.9073
0.005	4.5921e-05	1.0353e-04	1.9811
0.0025	1.1749e-05	2.6489e-05	1.9666

The example occupies the rectangle $\{-0.5 \text{ km} \le x_1 \le 0.5 \text{ km}, 0 \le x_3 \le 1 \text{ km}\}$; the source is located at $x_1 = 0.0$ km, $x_3 = 0.0$ km. The four Thomsen's parameters of homogeneous Zinc model are $\alpha_0 = 2.492$km/s, $\beta_0 = 2.000$km/s, $\epsilon = 0.7802$, $\delta = 2.6562$. According to the notion of Thomsen's weak anisotropy, these parameters show that the anisotropy is strong rather than weak. To obtain the ITI model, the rotation angle is 36 degrees.

The initial data depth is at $x_3 = 0.04$ km and the paraxial parameter Δ along depth direction is taken as 0.01. The results are shown on Table 1, where Δx_1 is the x_1 direction grid sampling, Δx_3 is the x_3 direction grid sampling (taken as $\Delta x_3 = 0.01$ km); the maximum absolute error Abs.Err and maximum relative error Rel.Err are measured at bottom $x_3 = 1$ km, where we use the solution from the analytical solver as true solutions; α is the estimated convergence order. A glance of the table shows that the scheme is of second-order accuracy.

Figures 2, 3 and 4 further illustrate the results computed by using DNO and PS techniques. The computational grid is 51 by 51; the DNO marching is performed by down marching first, followed by right and left marching.

Conclusions

In this paper we presented a second-order upwind scheme enhanced by DNO and PS update for computing the full-aperture traveltime field of quasi-P waves in general anisotropic media. Numerical experiments for Zinc model with strong anisotropy demonstrated the accuracy and efficiency of these algorithms. A fully adaptive eikonal solver based on a posteriori error estimates for general numerical methods of Hamilton-Jacobi equations (Albert et al.,) will be subject of a subsequent paper.

Acknowledgements

JLQ thanks Prof. Bernardo Cockburn and Colin Zelt for their interests in this research.

References

Albert, S., Cockburn, B., French, D., and Peterson, T., A posteriori error estimates for general numerical methods for Hamilton-Jacobi equations. part I: The steady state case: Math. Comp., **to appear**.

Cerveny, V., 1972, Seismic rays and ray intensities in inhomogeneous anisotropic media: Geophys. J. Roy. Astr. Soc., **29**, 1–13.

de Hoop, M. V., Spencer, C., and Burridge, R., 1999, The resolving power of seismic amplitude data: An anisotropic inversion/migration approach: Geophysics, **64**, 852–873.

Dellinger, J., and Symes, W. W., 1997, Anisotropic finite-difference traveltimes using a Hamilton-Jacobi solver: 67th Ann. Internat. Mtg., Soc. Expl. Geophys., Expanded Abstracts, 1786–1789.

Dellinger, J., 1991, Anisotropic seismic wave propagation: Ph.D. thesis, Stanford University, Stanford, CA94305.

Kim, S., and Cook, R., 1999, 3-D traveltime computation using second-order ENO scheme: Geophysics, **64**, 1867–1876.

Kim, S., 1999, Eikonal solvers for anisotropic traveltimes: 69th Ann. Internat. Mtg., Soc. Expl. Geophys., Expanded Abstracts, 1875–1878.

Musgrave, M. J. P., 1970, Crystal acoustics: Holden-Day.

Osher, S. J., and Shu, C. W., 1991, High-order Essentially NonOscillatory schemes for Hamilton-Jacobi equations: SIAM J. Num. Anal., **28**, 907–922.

Popovici, A. M., and Sethian, J. A., 1997, Three-dimensional traveltime computation using the fast marching method: 67th Ann. Internat. Mtg., Soc. Expl. Geophys., Expanded Abstracts, 1778–1781.

Qian, J., and Symes, W. W., 1999, Finite-difference quasi-P traveltimes for anisotropic media: Annual Report, The Rice Inversion Project, http://www.trip.caam.rice.edu/.

Qian, J., Belfi, C. D., and Symes, W. W., 1999, Adaptive finite difference method for traveltime and amplitude: 69th Ann. Internat. Mtg., Soc. Expl. Geophys., Expanded Abstracts, 1763–1766.

Qin, F., and Schuster, G. T., 1993, First-arrival traveltime calculation for anisotropic media: Geophysics, **58**, 1349–1358.

Schneider, W. A. J., Ranzinger, K., Balch, A., and Kruse, C., 1992, A dynamic programming approach to first arrival traveltime computation in media with arbitrarily distributed velocities: Geophysics, **57**, 39–50.

van Trier, J., and Symes, W. W., 1991, Upwind finite-difference calculation of traveltimes: Geophysics, **56**, 812–821.

Vidale, J., 1988, Finite-difference calculation of travel times: Bull., Seis. Soc. Am., **78**, 2062–2076.

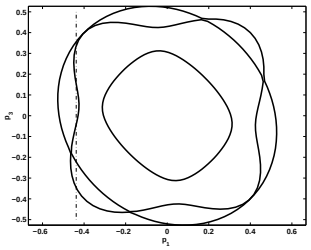

Fig. 1: The slowness surface for typical anisotropic media: a sextic surface which consists of three slowness sheets.

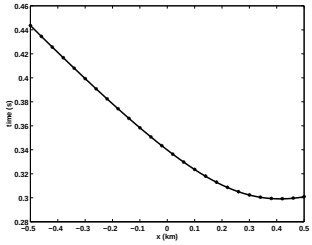

Fig. 2: The Zinc ITI model obtained by rotating VTI model 36 degrees: the analytical solution (solid line) vs. numerical solution (*) by DNO and PS. Before PS, Abs.Err is 0.0017 (s); after three PS, Abs.Err is 1.9584e-04 (s).

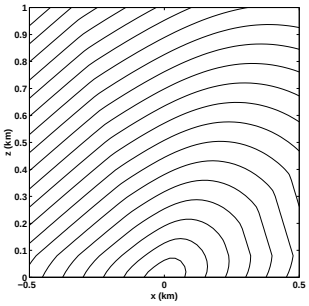

Fig. 3: The Zinc ITI model obtained by rotating VTI model 36 degrees: traveltime contours obtained by downgoing marching along depth direction only with paraxial parameter Δ=0.20.

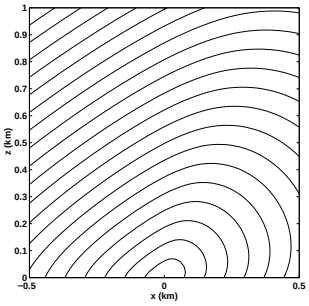

Fig. 4: The Zinc ITI model obtained by rotating VTI 36 degrees: traveltime contours by DNO and three PS. The paraxial parameter along depth is chosen to be 0.20; the paraxial parameter along x+ and x- direction is chosen to be 0.020.